

View Article Online
View Journal

Journal of Materials Chemistry C

Materials for optical, magnetic and electronic devices

Accepted Manuscript

This article can be cited before page numbers have been issued, to do this please use: L. Wang, Y. Hajee, J. Frimat, M. Diba and A. Savva, *J. Mater. Chem. C*, 2025, DOI: 10.1039/D5TC02708J.



This is an Accepted Manuscript, which has been through the Royal Society of Chemistry peer review process and has been accepted for publication.

Accepted Manuscripts are published online shortly after acceptance, before technical editing, formatting and proof reading. Using this free service, authors can make their results available to the community, in citable form, before we publish the edited article. We will replace this Accepted Manuscript with the edited and formatted Advance Article as soon as it is available.

You can find more information about Accepted Manuscripts in the <u>Information for Authors</u>.

Please note that technical editing may introduce minor changes to the text and/or graphics, which may alter content. The journal's standard <u>Terms & Conditions</u> and the <u>Ethical guidelines</u> still apply. In no event shall the Royal Society of Chemistry be held responsible for any errors or omissions in this Accepted Manuscript or any consequences arising from the use of any information it contains.



View Article Online DOI: 10.1039/D5TC02708J

Electrically Active Hydrogels Based on PEDOT:PSS for Neural Cultures

Liwen Wang¹, Yannick Hajee², Jean-Philippe Frimat³, Mani Diba², Achilleas Savva¹*

¹Department of Microelectronics, Faculty of Electrical Engineering, Computer Science and Mathematics, Delft University of Technology, Delft, the Netherlands

²Regenerative Biomaterials–Dentistry, Research Institute for Medical Innovation, Radboud University Medical Center, Nijmegen, the Netherlands

³Department of Human Genetics, Leiden University Medical Center, Leiden, the Netherlands

*E-mail: a.savva@tudelft.nl

Keywords: Electrically active hydrogels, PEDOT:PSS, Organic Bioelectronics

Abstract

Open Access Article. Published on 28 Oktoba 2025. Downloaded on 17/11/2025 01:06:17.

Electrically active hydrogels are attracting significant interest as biohybrid materials for electrical interfacing with biological tissues. Here, we report the development of electrically active hydrogels, specifically engineered for *in vitro* neural cell cultures. The hydrogels' matrix comprises a viscoelastic alginate primary network, interpenetrated by a secondary network formed by the neural cell-adhesive protein, laminin. Conducting poly(3,4-ethylenedioxythiophene):polystyrene sulfonate (PEDOT:PSS) particles are embedded throughout the hydrogel matrix, serving as the electrically active filler phase. Oscillatory rheology confirmed the viscoelastic nature of the composite hydrogels, with storage and loss moduli in the range of 1–10 kPa, suitable for neural tissue interfacing. The hydrogels exhibited high optical transparency across the visible spectrum. At a wavelength of 500 nm, transmission exceeded 45% for 400 µm thick hydrogels, and was further enhanced to over 60% by reducing the hydrogel thickness to 150 µm. We established a reproducible protocol for electrochemical impedance spectroscopy and cyclic voltammetry measurements, demonstrating that incorporation of PEDOT:PSS significantly enhanced both conductivity and charge storage capacitance of hydrogel films. The Alginate-Laminin-PEDOT:PSS hydrogels demonstrated excellent operational stability, maintaining consistent electrochemical performance over 80 charging/discharging cycles and remaining structurally and functionally stable under cell culture conditions for over two weeks. Cortical neuron cultures derived from human induced pluripotent stem cells, prove the stability and cytocompatibility of our proposed hydrogels for over 28 days in culture. Collectively, these results highlight the potential of electrically active hydrogels loaded with PEDOT:PSS as soft, bioelectronic interfaces for neural engineering applications.

IntroductionView Article OnlineDOI: 10.1039/D5TC02708J

Bioelectronic materials and devices are emerging as promising platforms for monitoring and stimulating *in vitro* cell cultures.^{1,2} These platforms have advanced our understanding of complex biological processes associated with neuron electrophysiology and guided the development of future clinical treatments.³ Conventional bioelectronic *in vitro* models are based on 2D cell cultures—where a cell monolayer is formed and adhered to protein-coated microelectrode arrays.^{4,5} However, these systems fail to replicate the physical and chemical complexity of the human biology, and often result in cells with different functionality compared with cells that grow *in vivo*.¹

3D human-like *in vitro* systems have been proven crucial for stem cell engineering and neuron regeneration. These systems have significantly benefited from the development of soft biomaterials, and particularly hydrogels. Such biomaterials can replicate the mechanical properties of neural tissue (i.e. soft with young's moduli ~1 kPa) and deliver biochemical cues that are crucial for neural growth in the body. Hydrogels made of extracellular matrix (ECM) components, or blends with other polymeric materials such as alginate, have been extensively used to develop biomimetic 3D neural cultures. These hydrogels provide a supportive environment that mimics the natural cellular surroundings, which is crucial for studying neural behavior and developing effective disease treatments. Alginate-based hydrogels can be fine-tuned by controlling molecular weight of alginate chains as well as crosslinking density to produce hydrogels with adjustable viscoelasticity, rendering them excellent biomaterial candidates for *in vitro* 3D neural cultures. 10,11

More recently, electrically active hydrogels are gaining attention due to their ability to replicate the bioelectrical patterns of neural tissue, while preserving excellent mechanical and chemical compatibility. These biohybrid electronic materials can be tailored to construct highly biomimetic electrodes for neural recordings, and injectable conducting hydrogels for spinal cord injuries. Helectrically active hydrogels for 3D *in vitro* models was found to enhance the differentiation and maturation of stem cells towards neural lineage, due to the hydrogel's inherent electrical properties. These results are highly promising and demonstrate how further development of electrically active hydrogels can be optimized to guide the differentiation and maturation of stem cells into neural tissue, opening new opportunities for bioelectronic applications in neural engineering. The most commonly used strategy to render hydrogel matrices electroconductive is by blending electroconductive particles with hydrogel forming polymers, such as alginate and gelatin. Conducting materials such as carbon nanotubes, graphene, and silver nanowires have been used to create conducting hydrogels that can support the development of 3D neural cultures, *in vitro*.

Electrically active hydrogels made with the conducting polymer PEDOT:PSS (i.e. Poly(3,4-ethylenedioxythiophene) polystyrene sulfonate) are gaining attention.^{20,21} The chemistry of PEDOT:PSS and it's stable water dispersions that are commercially available in large quantities provide

flexibility in preparation and casting of highly cytocompatibility hydrogels, with tunable properties dispersed in a gelatin methacryloyl (GelMA) matrix to obtain an electrically active hydrogel system with cells encapsulated, proving its potential in 3D tissue guidance through electrical stimulation.²² Recently, Rutz et al. showed the development of 3D printable PEDOT:PSS-based hydrogel with an ionic liquid as a cross-linker.²³ The excellent cytocompatibility of PEDOT:PSS is already demonstrated in several studies that developed electronic scaffolds able to host 3D human stem cell²⁴ and neural cultures.²⁵

Here, we show the development of electrically active hydrogel systems made with a combination of PEDOT:PSS embedded in a viscoelastic matrix formed by sodium alginate and supported by a secondary network of the neural protein laminin. A comprehensive analysis of the hydrogels' key properties is presented, confirming their excellent compatibility with the demands of sensitive stem cell–derived neural cultures. We show that high optical transparency in the visible spectrum can be maintained even after the PEDOT:PSS particle inclusion in the hydrogel matrix, which can be further fine-tuned by controlling the thickness of the hydrogels in the range between 150 µm and 400 µm. Furtehrmore, we examine in detail the mechanical properties of the hydrogels with oscillatory rheology. The storage moduli (G') of the hydrogels with PEDOT:PSS are shown to be in the range of 5 kPa, which verifies the compatibility of the hydrogels with the mechanical properties of neural tissue. ²⁶ Detailed electrochemical characterization reveals an increase in electrical conductivity and charge storage capacitance of the hydrogels containing PEDOT:PSS compared with pure-alginate/laminin hydrogels, and stable electrochemical operation for more than 80 charging cycles. Finally, the hydrogels are highly stable in stem cell cultures conditions for more than 28 days, and highly biocompatible as proved by live/dead assays of cortical neurons derived from human induced pluripotent stem cell cultures.

Results and discussion

The electrically active hydrogels were made by mixing the water dispersion of PEDOT:PSS with water solutions of alginate and laminin, and casting them in tailor-made molds with controlled thickness, as described in the experimental section. A schematic of Alginate-Laminin-PEDOT:PSS hydrogel network is illustrated in Figure 1. The sodium alginate forms the primary network of the hydrogel upon crosslinking with Ca²⁺ ions.^{27,28} To prove the formation of the laminin interpenetrating network we used a laminin tagged with a fluorescent label (i.e. Red Fluorescent, Rhodamine – see experimental section) and imaged the electrically active hydrogels with fluorescence microscopy. As shown in Figure 1 a uniform fluorescence distribution across a wide surface is observed, proving the stable formation of the laminin network within the hydrogel. The conducting PEDOT:PSS particles, are expected to be entangled within this interpenetrating network formed by alginate and laminin, forming partially connected electrically conducting networks. Following this understanding, we fine-tuned the casting and gelation process of the hydrogels by using slowly-dissolving CaSO₄ particles to control the release rate of calcium ions.^{27,29} This approach prevents excessively fast gelation, and allows for the

controllable casting of the hydrogels in custom made 3D printed molds of different shapes in custom made 3D printed molds of different shapes in the height of the molds, different hydrogel thicknesses can be achieved, spanning from 150 µm to 10 mm.

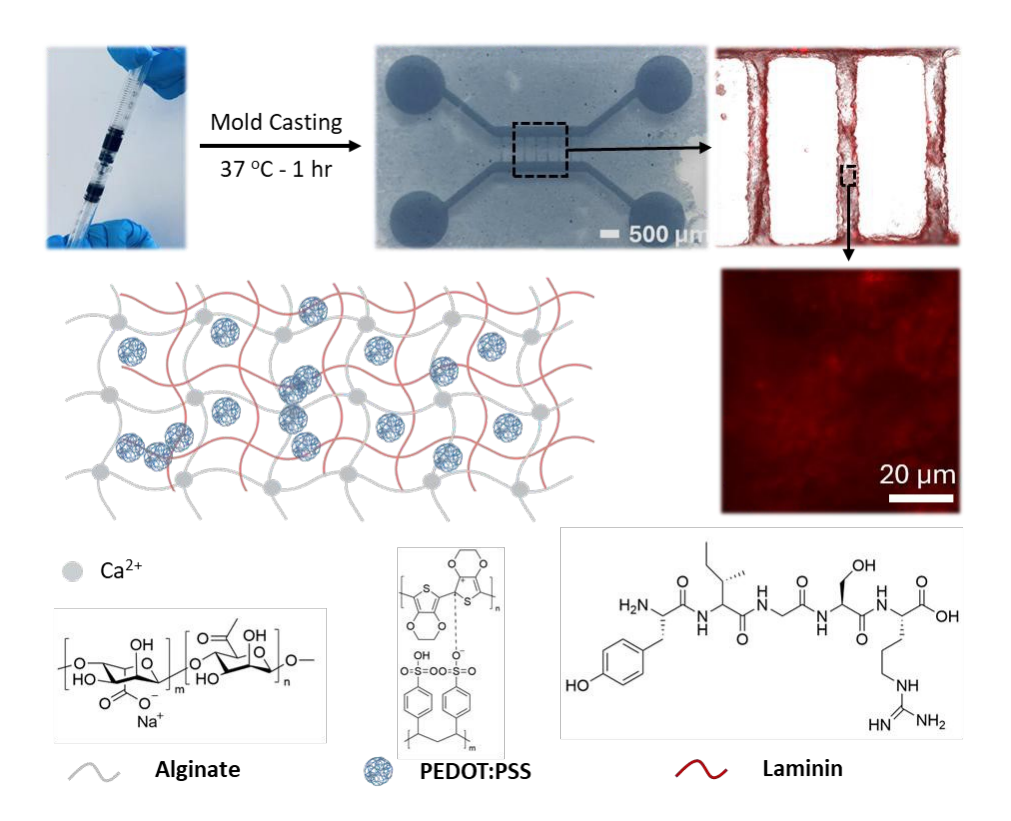


Figure 1: A schematic representation of the Alginate-Laminin-PEDOT:PSS hydrogel system with an interpenetrating network forming and PEDOT:PSS nanoparticles included in the matrix. The particles are partially percolated, forming electrically active pathways within the ionically conducting hydrogel matrix. The top row illustrates the preparation process, where two syringes are interconnected using a luer-lock connector to mix the hydrogel precursors— the first one contains the sodium alginate and laminin and the water dispersion of PEDOT:PSS – and the second contains the CaSO₄ to initiate gelation upon casting at 37 °C in custom-made molds. The top row also includes a digital image of the patterned hydrogel and a fluorescence image showing laminin distribution.

To evaluate the properties of the hydrogels we performed a number of characterization techniques. We focused on hydrogels with a controlled thickness of 400 µm made with two different concentrations of PEDOT:PSS - i.e. 0.9 and 1.2 wt%, referred as Alg-Lam-PEDOT:PSS 0.9 and Alg-Lam-PEDOT:PSS 1.2, respectively. For comparison we used pure Alginate—Laminin hydrogel, referred as Alg-Lam. First, we focused on the optical properties of the hydrogels and the results are shown in Figure 2. Transparency is crucial for *in vitro* neural cultures since it allows high resolution microscopy to be performed. The digital pictures of all the formulations studied are shown in Figure 2a. Although the inclusion of PEDOT:PSS in the hydrogels reduces transparency in the wavelength range of 300 – 800 cm⁻¹, the Alg-Lam-PEDOT:PSS 0.9 maintains good transparency in the visible spectrum – a useful property for high resolution microscopy of neural cultures. These results were quantified via optical

transmittance measurements as shown in Figure 2b. The transparency of Alg-Lam-PEDOT:PSS $^{\circ}_{10.1039}/^{\circ}_{0.5102708J}$ hydrogel at λ =500 nm was found to be 45.95%, and 19% for the Alg-Lam-PEDOT:PSS 1.2 hydrogel. These transmittance values can be controlled by tuning the thickness of the hydrogels, as shown in Figure S1. We found that the transmittance of the Alg-Lam-PEDOT:PSS 0.9 can be increased to 64%, at λ = 500 nm, by reducing the thickness from 400 μ m to 150 μ m. Similarly, the transmittance of the Alg-Lam-PEDOT:PSS 1.2 hydrogel can be increased to 35%. These results show that highly transparent electrically active hydrogels can be achieved despite the inclusion of the conducting polymer, which can be beneficial for *in vitro* neuron culture studies.

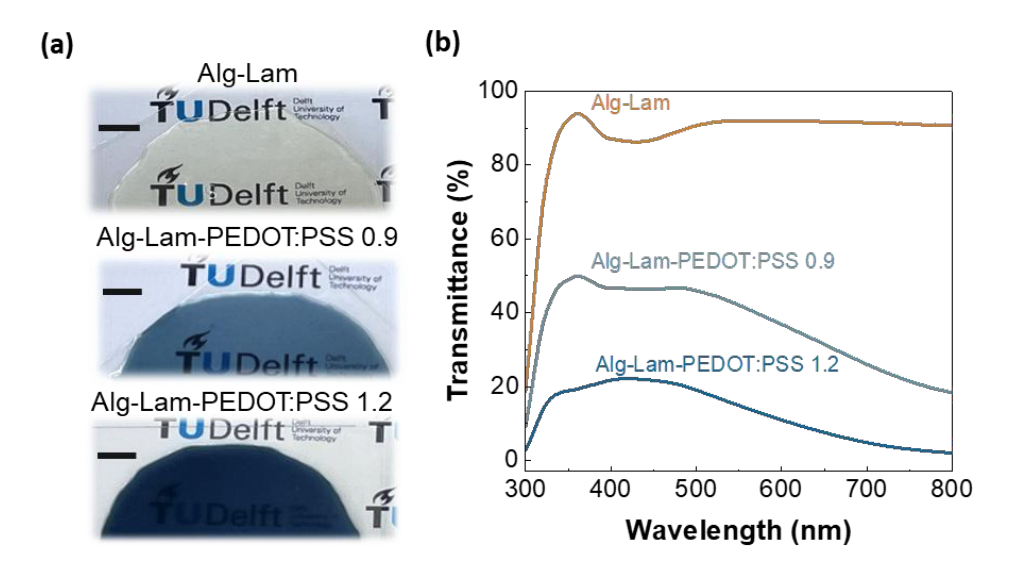


Figure 2: a) Digital pictures of the different hydrogels studied with thickness of 400 μm. Scale bars = 1 mm. b) Optical transmittance of the Alg-Lam (orange line), Alg-Lam-PEDOT:PSS 0.9 (light blue line) Alg-Lam-PEDOT:PSS 1.2 (blue line) hydrogels with thickness of 400 μm.

Next we moved on to the characterization of the viscoelastic properties of the hydrogels – an important aspect for highly biomimetic neural cultures due to the viscoelastic properties of neural tissue. 30,31 These properties were evaluated with oscillatory rheology and the results are shown in Figure 3. Oscillatory time sweep tests were first applied to verify the gelation of alginate, Alg-Lam and Alg-Lam-PEDOT:PSS hydrogels. Due to the fast gelation of the alginate network, the crossover points were difficult to observe (Figure S2). However, as shown in Figure S2, the storage modulus (G') was consistently higher than loss modulus (G"), which proved the formation of the hydrogels. There was no significant change in G' and G" over the measurement period, indicating complete gelation stability for all compositions of the material and the final values are shown in Figure 3a. The alginate only hydrogel showed an average G' of 4.59 kPa at a fixed frequency of 1 Hz, similar to Alg-Lam hydrogels (i.e. 5.74±0.92 kPa). However, we found that G' is reduced when PEDOT:PSS particles are incorporated in the hydrogel matrix, with Alg-Lam-PEDOT:PSS 0.9 measured at 1.74±1.22 kPa and Alg-Lam-PEDOT:PSS 1.2 measured at 1.48±0.83 kPa. To further evaluate the degree of solid-like response of

the hydrogels, we also evaluated the damping factor as shown in Figure 3a bottom panel (i.e. $G'/G^{\text{tow}} \wedge G^{\text{picle Online}}$) often found in literature as $\tan(\delta)$). We found that for all of our hydrogel formulations the damping factor remained within a range of 0.2 and 0.4, with a slight increase for the hydrogels that include PEDOT:PSS. This proves that the viscoelastic properties of the material are dominated by the alginate network and slightly influenced by the inclusion of PEDOT:PSS.

The viscoelastic nature of the hydrogels is further evaluated with stress relaxation measurements as shown in Figure 3b, which is a critical property for interfacing hydrogels with stem cell cultures.³² Stress relaxation reflects how quickly internal stresses in a material dissipate upon applying a fixed deformation; the relaxation half-time is the time to reach 50% of the initial stress. The impact of the hydrogel's stress relaxation profile on cells is context-dependent. In various 3D culture systems, faster-relaxing hydrogels allow cells to remodel their surroundings more readily and are typically associated with increased spreading and migration when other cues (e.g., elastic modulus, ligand density) are held constant.^{33,34} As shown in Figure 3b, the half-time relaxation is reduced when PEDOT:PSS particles are included in the hydrogel's matrix. Sulfonate groups have been reported to bind strongly to sodium alginate.³⁵ Accordingly, we propose that the observed reduction in stress relaxation with increasing PEDOT:PSS concentration likely results from the disruption of the Ca²⁺-mediated alginate network by the sulfonate-rich PSS phase. This disruption, likely due to competition for Ca²⁺ ions and electrostatic screening, decreases the effective crosslink density of the hydrogel network and facilitates accelerated stress relaxation.

As shown in Figure 3c, all hydrogel compositions studied showed a G' and G" that were mostly constant across a range of frequencies (1 - 100 rad/s) – indicating frequency independent solid-like behavior. The differences in yielding behavior across compositions, were also examined and the measurements are shown in Figure 3d. The yield strain was extracted by identifying the crossover point of G' and G" (from Figure 3d). Yield strain is the critical strain at which the material transitions from elastic (reversible deformation) to plastic (irreversible deformation) behavior. For hydrogel matrices employed for cell culture, a lower yield strain implies that plastic remodeling initiates at smaller deformations, which can facilitate cell extension and network reorganization when other cues (e.g., modulus, ligand density) are held constant. Conversely, lower yield strain typical indicates inferior mechanical stability for long-term structural retention of the hydrogel, emphasizing that the preferred yield strain is context depended. We found that the inclusion of PEDOT:PSS has a significant effect on the yield strain of the hydrogels which was found at 91.74%, 110.44±7.86%, 35.19±13.44%, 11.53±7.01% and for Alg, Alg-Lam, Alg-Lam-PEDOT:PSS 0.9 and Alg-Lam-PEDOT:PSS 1.2 respectively. We propose that the observed reduction in yield strain is likely due to competition for Ca²⁺ ions and electrostatic screening of PSS sulfonate groups in PEDOT:PSS particles. Moreover, the PEDOT:PSS particles embedded within the hydrogel matrices do not form strong inter-particles crosslinks even above their percolation threshold. Therefore, PEDOT:PSS domains within the hydrogels likely act as compliant, weak wide Courses coupled inclusions that facilitate interfacial slip and early yielding under increasing strain levels.

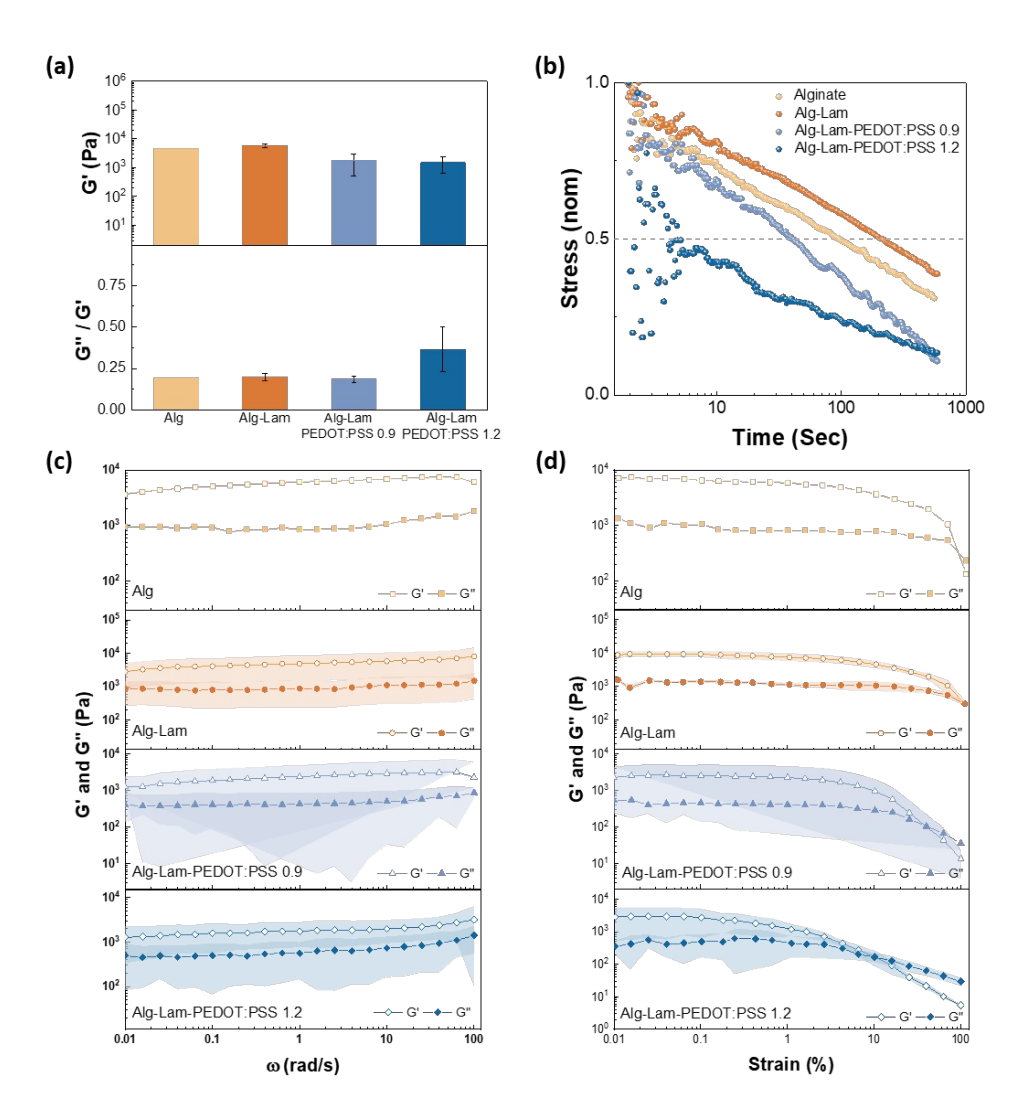


Figure 3: a) The storage modulus (G') and the damping factor (i.e. $\tan (\delta) = G''/G'$) measured at strain 0.5% at $\omega=1$ Hz. b) Stress relaxation profiles for all the hydrogels developed in this study. c) Frequency sweep from 0.01 - 100 rad/s at 0.05% strain and d) strain sweep from 0.01 - 100% at 1 rad/s.

Optical transmittance and oscillatory rheology measurements proved that the hydrogels can be rendered transparent, soft, and viscoelastic – important parameters for neuron cultures. The electrochemical characterization of hydrogels was investigated with electrochemical impedance spectroscopy (EIS) and cyclic voltammetry (CV), using a custom made setup shown in Figure 4a, and supplementary Figure S3. 3D printed molds with fixed dimensions (i.e. length=5 mm * width=5 mm * height=10 mm) were used and the hydrogels were directly casted in, with a controlled thicknesses of 10 mm. An integrated gold pogo pin allows for stable gold/hydrogel contacts and accurate evaluation of the electrochemical operation of the hydrogels, with reliable results across samples. Our initial trials to measure the electrochemical properties of the hydrogels by simply casting the hydrogels on gold or indium-tin-oxide

flat substrates did not yield reliable results due to the weak adhesion of the soft hydrogels on the verbidice online electrodes, resulting in delamination and inconsistent readings (Figure S4). In our approach, we kept all the parameters of the measurements constant, with the only changing parameter being the PEDOT:PSS concentration in the hydrogels. The samples were immersed in cell media overnight to ensure homogeneity in swelling and a reference (Ag/AgCl) and a counter (Pt mesh) electrodes were used to measure EIS and CV. The cell culture medium used was Dulbecco's Modified Eagle's Medium (DMEM), containing amino acids, vitamins, and glucose, and maintained at a physiologically relevant pH of 7.4. The same medium was employed during hydrogel formation, and its use in electrochemical measurements ensured the stability of the hydrogel system by minimizing osmotic effects arising from differences in concentration and composition between the hydrogel and the cell culture environment. Such a system is highly customizable and allows for measurements under consistent hydration conditions.

The impedance magnitude over a range of frequency (i.e. 10^5 Hz - 0.1 Hz) of the hydrogels was extracted from EIS measurements and is shown in Figure 4b, and the mixed ionic electronic conduction properties of the hydrogels can be evaluated by looking at the different frequency bands of the impedance. As recently suggested by Daso et al., 36 the impedance spectra of a hydrogel system with electrically conducting nanoparticle fillers can be simulated with an equivalent circuit to distinguish ionic and electronic conductivities. As it is also reported elsewhere, the high frequency band (>10⁴ Hz) is dominated by the fast ionic movement in the hydrogels and low frequency band (<10 Hz) is dominated by the electronic conductivity and the interaction of the electronic current with the ionic current within the hydrogels.³⁷ Therefore, we were able to extract the ionic and electronic conductivities of the different hydrogel systems by simply using the resistance values at f=10⁵ Hz and at 0.1 Hz, respectively from the resistance (i.e. real part of impedance) versus frequency plot in Figure S5. The ionic and electronic conductivities were then extracted using equation 2 (see experimental section). No significant changes in the ionic conductivity values were observed for the different systems under study - i.e. ionic conductivity of 1.6*10⁻⁴; 1.3*10⁻⁴; 2*10⁻⁴ S/m for the Alg-Lam, Alg-Lam-PEDOT:PSS 0.9, and Alg-Lam-PEDOT:PSS 1.2, respectively. However the electronic conductivity of hydrogels loaded with PEDOT:PSS increases by approximately 10 times compared with the hydrogels with no PEDOT:PSS loading – i.e. 2.9*10⁻⁴; 1.9*10⁻³; 4.1*10⁻³ S/m the Alg-Lam, Alg-Lam-PEDOT:PSS 0.9, and Alg-Lam-PEDOT:PSS 1.2, respectively. These results suggest that our hydrogel system comprises PEDOT:PSS particles stably embedded within the hydrogel matrix, with partially developed percolation pathways that enable electron conduction. These percolation pathways appear to be better interconnected in Alg-Lam-PEDOT:PSS 1.2 compared to Alg-Lam-PEDOT:PSS 0.9, as evidenced by a slight increase in electronic conductivity from 1.9 to 4.1×10^{-3} S/m. However, this increase was not statistically significant, as variations were observed across samples, as shown by the shaded regions around each main line in Figure 4b for the hydrogels studied. The statistical error bars were calculated from five samples in each case, and similar trends were confirmed in multiple independent experimental

batches. These findings suggest that the percolation network is already well established at a 0.9 Very officie Online PEDOT:PSS loading, and that a further increase of 0.3 wt% provides limited enhancement in pathway development. Interestingly, as observed in Figure 2, increasing the loading to 1.2 wt% notably reduces the transparency of the hydrogels while providing minimal gains in electronic conductivity—an important design consideration for subsequent cell culture studies. This hypothesis and interpretation are illustrated schematically in Figure 1.

Importantly, we were able to also clearly observe a capacitance increase for the hydrogels loaded with PEDOT:PSS compared with the pure Alg-Lam hydrogel. From the capacitance vs frequency plots in Figure S5, we found that the value of the capacitance at 0.1 Hz is at 2.9*10⁻⁶, 4.2*10⁻⁵, and 7.5*10⁻⁵ F for the Alg-Lam, Alg-Lam-PEDOT:PSS 0.9, and Alg-Lam-PEDOT:PSS 1.2, respectively. This represents more than 10 times increase when 1.2 wt% of PEDOT:PSS is loaded in the pure Alg-Lam hydrogel network. These results show that PEDOT:PSS particles can attract charge and render the hydrogel electrically active, even without fully developed percolation networks for optimum electronic conductivity.

The capacitive properties of the hydrogel loaded with PEDOT:PSS were further verified with cyclic voltammetry as shown in Figure 4c. By integrating the graph area enclosed by the CV for each of the hydrogel systems, and applying equation 3 (see experimental section) we calculated the capacitance value at 5.8*10⁻⁶, 3.4*10⁻⁵ and 5.2*10⁻⁵ F for Alg-Lam, Alg-Lam-PEDOT:PSS 0.9 and Alg-Lam-PEDOT:PSS 1.2 respectively. Here we note that the scan rate we use for the CV measurements (i.e. 0.1 V/s) corresponds to an equivalent frequency of 0.2 Hz, according to the equation 4 (see experimental section), and therefore the values of capacitance are in line with the capacitance extracted from the EIS at 0.1 Hz, and verify the accuracy of our measurements and our analysis. We have also studied CVs at different scan rates as shown in Figure S6, where we observe increased capacitance of the hydrogels that include PEDOT:PSS at all scan rates studied, verifying the stable inclusion of the electroactive particle of PEDOT:PSS within the alginate/laminin hydrogel network. We were able to calculate the volumetric capacitance (C^*) using the capacitance values extracted from Figure 4c. The fixed sample volume was accurately defined by the dimensions of the 3D-printed molds and the reproducible hydrogel thickness (i.e. 0.25 cm^3). Based on these parameters, the calculated C^* for the various hydrogel systems was found at 2.32*10⁻⁵, 1.36*10⁻⁴, 2.07*10⁻⁴ F/cm³, respectively. All the properties of the different hydrogels under study are summarized in table 1.

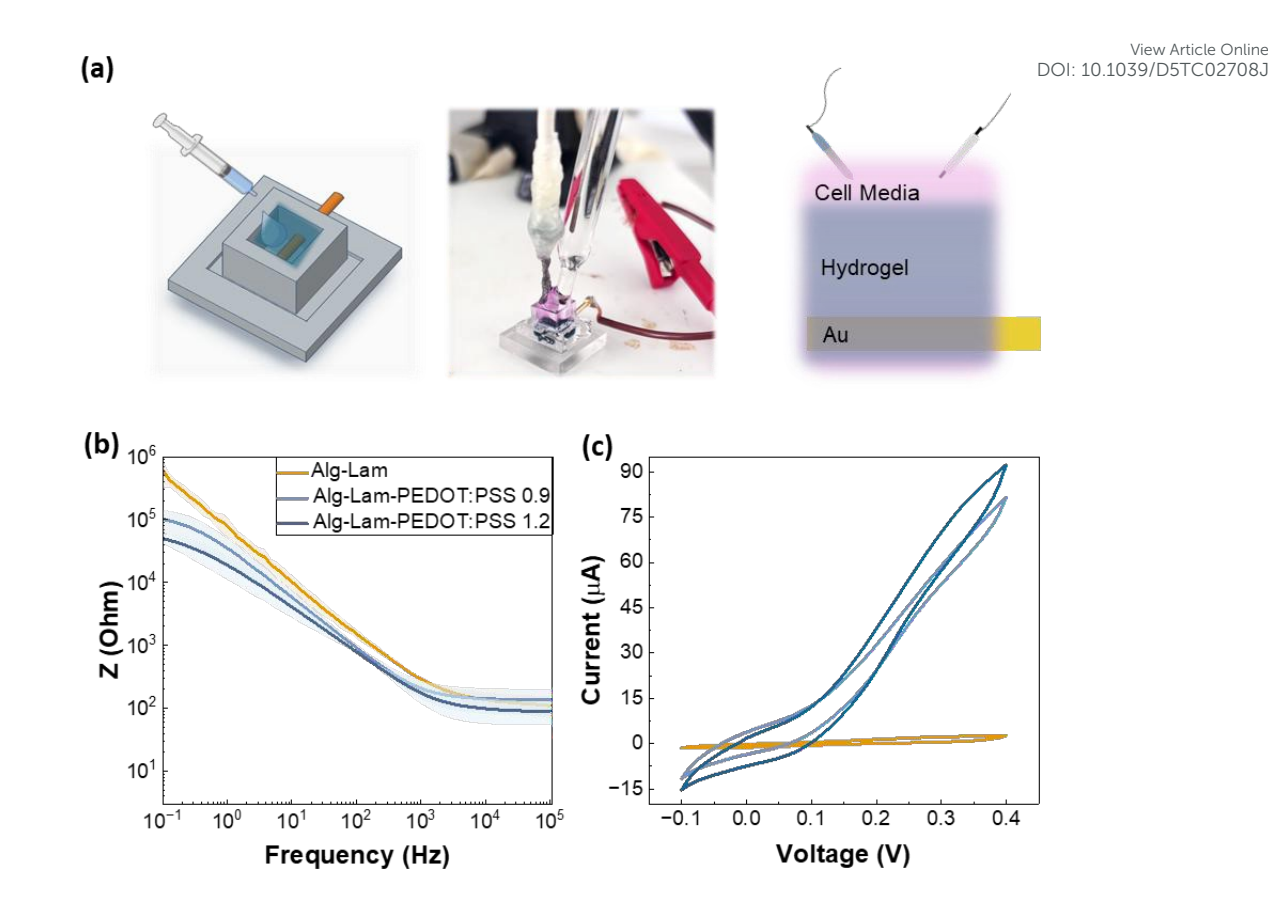


Figure 4: a) Schematic and digital picture of the electrochemical setup developed to probe the properties of the hydrogels and suggested equivalent circuit. A custom made 3D printed mold (L=5 mm*W=5 mm H= 10 mm) with an integrated gold pogo pin encapsulated in the hydrogels of 1 cm thicknesses. All measurements were performed in cell culture media (DMEM/F12 – pH 7.4) at 37°C, with the support of an Ag/AgCl reference and a Pt mesh counter electrode immersed fully in the electrolyte. The shaded areas around the lines represent the statistical error bars for each condition obtained from 5 samples. **b)** The impedance magnitude versus frequency plots obtained with electrochemical impedance measurements for Alg-Lam (orange lines), Alg-Lam-PEDOT:PSS-0.9 (light blue lines) and Alg-Lam-PEDOT:PSS-1.2 (blue lines). 3 samples were measured in each case. **c)** Cyclic voltammograms of the different hydrogels studied, obtained with a scan rate of 0.1 V/s.

Table 1: Summary of the key properties measured for the hydrogels developed in this study.

	Transmittance at λ =500 nm (%) $d = 400 \mu m$	G' (kPa) d = 500 μm	G''/G' $d = 500 \text{ μm}$	Electronic Conductivity - EIS @ 0.1 Hz S/m $d = 10 \text{ mm}$	Capacitance $- EIS @ 0.1$ Hz (F) $d = 10 \text{ mm}$	Capacitance - CV (F) $d = 10 \text{ mm}$	C* - CV (F/cm ³)
Alg-Lam	90 %	5.74	0.2	2.9*10-4	2.9*10-6	5.8*10-6	2.32*10 ⁻⁵
Alg-Lam- PEDOT:PSS 0.9	46 %	1.74	0.19	1.9*10 ⁻³	4.2*10 ⁻⁵	3.4*10 ⁻⁵	1.36*10-4

Open Access Article. Published on 28 Oktoba 2025. Downloaded on 17/11/2025 01:06:17.

Alg- Lam –						View Article Online DOI: 10.1039/D5TC02708J	
PEDOT:PSS 1.2	19 %	1.48	0.37	4.1*10 ⁻³	7.5*10 ⁻⁵	5.2*10 ⁻⁵	2.07*10 ⁻⁴
							-

The detailed optical, mechanical and electrochemical characterization showed promising results for interfacing the electrically active hydrogels with neural tissue. To further evaluate the potential of the materials for neural cultures we performed a series of experiments. First, we measured the changes in pH in the cell media after incubating the hydrogels for over 48 hours, to assess potential release of acidic PEDOT:PSS particles. The pH was measured at 7.82 when incubated with Alg-Lam-PEDOT:PSS hydrogels for 48 hours, compared to pH 7.77 in the control media. These results were verified with 5 samples in each case, and indicate that no PEDOT:PSS particles are leaching out of the hydrogels.

To further support these observations, we found that the electrically active hydrogels preserved their shape and size over four weeks when immersed in cell media and exposed in a cell incubator (Figure S8). We note that different concentrations of PEDOT:PSS were used for these experiments, ranging from 0.3 - 1.2 wt% with identical results obtained in all cases. All cell culture data presented in this study are obtained with an electrically active hydrogel with 0.6 wt% concentration of PEDOT:PSS loaded in the hydrogel matrix. The electrochemical properties of electrically active hydrogels loaded with 0.6 wt% PEDOT:PSS were similar with the hydrogels loaded with 0.9 wt% PEDOT:PSS as shown in Figure S9. To further evaluate the cytocompatibility of the electrically active hydrogels, we used SH-SY5Y cell cultures growing alongside the different hydrogel formulations – a model neuroblastoma cell line that is widely used in *in vitro* neural culture studies. As shown in Figure S9 after 7 days *in vitro* the cells adhere, proliferate and start differentiating on all well plates regardless of the concentration of PEDOT:PSS. Live/dead assays revealed that the cell viability was over 90% in all cases (Figure S9), proving the non-cytotoxic nature of the hydrogels.

Lastly, we have incubated our electrically active hydrogels with cortical neurons derived from human induced pluripotent stem cells (hiPSCs). The hydrogels are stable and maintain their shape and integrity (Figure S10) during the whole duration of the neuron differentiation and maturation timeline which spans over 28 days as shown in Figure 5. Live/dead assays performed to the cell cultures growing alongside the hydrogels at day 28, revealed excellent cell viability for the cells as shown in Figure 5 (b – d). We calculated 86.43%, 94.98% and 94.74% cortical neurons viability when cultured in control conditions, alongside Alg-Lam hydrogel and alongside Alg-Lam-PEDOT:PSS hydrogel, respectively. These results clearly show that our proposed electrically active hydrogels are biocompatible and suitable for long term, hiPSCs differentiation protocols. To better identify the quality of our cortical neural culture, we performed immunofluorescence imaging on cultures at day 28 *in vitro*. All cultures were stained with the nuclei marker DAPI (blue) and the neuronal marker βIII-tubulin (green), as shown

in Figure 5. Both the cortical neurons that have been matured alongside the hydrogels with and with office online PEDOT:PSS show comparable cell density, neurite population and network formation, showing that the PEDOT:PSS inclusion in the hydrogels do not disrupt the delicate processes of neuronal differentiation and maturation. Here, it is worth noting that our proposed hydrogels are designed for future 3D encapsulation of hiPSCs and the development of 3D neural networks. The highly tunable nature of the electrical activity of our designed hydrogel system will allow for fundamental understanding of the effects of electrical cues on 3D stem cell growth into functional neural networks. However, it is well established that alginate-based hydrogels must be functionalized with the arginine–glycine–aspartate (RGD) peptide, as cells do not adhere or proliferate in its absence. ³⁹ Because our alginate system was not functionalized with RGD, establishing 3D cell encapsulation protocols was not feasible. Nevertheless, our results clearly demonstrate the structural integrity and cytocompatibility of the proposed electrically active hydrogels for long-term hiPSC-derived neural cultures, highlighting their potential for future 3D neural network development upon alginate functionalization.

This article is licensed under a Creative Commons Attribution 3.0 Unported Licence.

Open Access Article. Published on 28 Oktoba 2025. Downloaded on 17/11/2025 01:06:17.

View Article Online

DOI: 10.1039/D5TC02708J

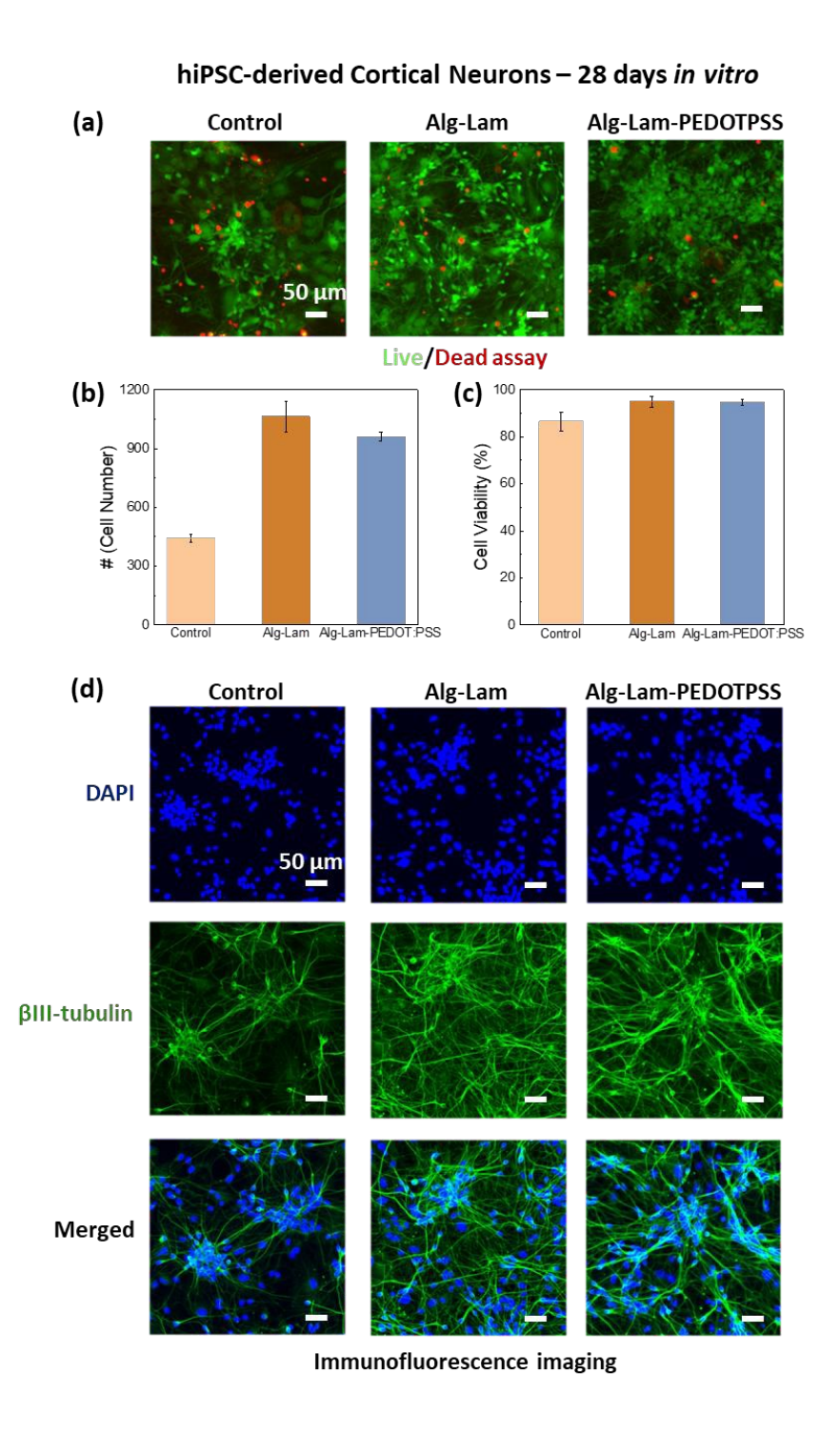


Figure 5: a) Live/Dead staining of hiPSC-derived cortical neurons on Day 28 *in vitro*. From left to right - control cultures grown on polystyrene well plates, on polystyrene well plates together with Alg-Lam hydrogels and on polystyrene well plates together with Alg-Lam-PEDOT:PSS hydrogels. **b)** Average live cell count and **c)** percentage of cell viability of hiPSC-derived cortical neurons directly exposed to the alginate-laminin and alginate-laminin-PEDOT:PSS hydrogels. **d)** Immunofluorescence imaging of hiPSC-derived cortical neurons cultures stained with the nuclear marker DAPI (blue) and the neuronal maker βIII-tubulin (green) on day 28 *in vitro*. Scale bars = 50 μm.

Conclusion View Article Online
DOI: 10.1039/D5TC02708J

We demonstrated the fabrication of electrically active hydrogels tailored for *in vitro* neural cultures, by integrating a viscoelastic alginate matrix interpenetrated with the neural protein laminin and embedded with conductive PEDOT:PSS particles. The electrically active hydrogels were prepared by mixing commercially available PEDOT:PSS dispersions, without any modification, with alginate and laminin solutions and casting them in custom 3D-printed molds, where slow Ca²⁺ release from CaSO₄ ensured uniform gelation and precise control over the hydrogel thickness. Detailed optical, mechanical, and electrochemical analyses revealed a combination of properties highly suited for neural cell cultures, supporting the use of these electrically active hydrogels as ideal materials for future biohybrid electronic interfacing of neural tissue. Optical transmittance measurements demonstrated good transparency across the visible spectrum, which can be finely tuned by adjusting the PEDOT:PSS concentration and hydrogel thickness. Transmittance values exceeding 60% at $\lambda = 500$ nm were achieved for $150 \mu m$ thick hydrogels. This is a key feature for high-resolution optical microscopy assessment of neural cultures, which is often overlooked in the design of similar biohybrid systems. In addition, we demonstrated that the hydrogels possess suitable mechanical properties for neural interfacing, with storage and loss moduli in the range of 1-10 kPa. Oscillatory rheology measurements and analyses, showed that hydrogels containing PEDOT:PSS particles show shorter relaxation half-times, suggesting a more dynamically permissive matrix for neural remodelling. Importantly, we developed an electrochemical setup to reproducibly characterize the electronic and ionic conduction within the electrically active hydrogels. Electrochemical impedance and cyclic voltammetry measurements showed that the inclusion of PEDOT:PSS within the hydrogel matrix, enhanced electrical conductivity and charge storage capacitance, with good operational stability over 80 electrochemical cycles. These results show that PEDOT:PSS particles are stably integrated within the hydrogel matrix, and can form partial percolation pathways to attract charge and render the hydrogel electrically active. We examined PEDOT:PSS loadings from 0.6 to 1.2 wt%, representing the maximum concentration attainable from commercial dispersions without modification. While higher loadings slightly improved electronic conductivity and charge storage capacitance, they also caused a substantial loss in optical transparency, underscoring the need to balance electrical and optical performance in bioelectronic hydrogel systems. Finaly, we found that the proposed electrically active hydrogels are highly compatible with cell cultures. The hydrogels demonstrated excellent stability under cell culture conditions for more than 28 days when maintained with human induced pluripotent stem cell-derived cortical neurons. As demonstrated by live/dead assays, the cultures show no distinct differences between the different hydrogel systems, indicating the highly cytocompatible nature of the proposed electrically active hydrogels.

To conclude, we developed electrically active hydrogel systems that combine desirable optical, mechanical, electrical, and cytocompatible properties for stem cell cultures. The tuneable nature of this system enables its future use as an electrically active scaffold to support and guide the growth of highly biomimetic three-dimensional neural cultures derived from human stem cells. Our findings position

Open Access Article. Published on 28 Oktoba 2025. Downloaded on 17/11/2025 01:06:17.

electrically active hydrogels based on PEDOT:PSS as versatile biohybrid platforms for next-general pla

Experimental

Materials: PEDOT:PSS (Clevios PH 100) was purchased from Heraeus, Germany. Sodium alginate (PRONOVA® UP VLVG, product NO. 42000001) with molecular weight (Mw) less than 75 kDa, dulbecco's modified eagle's media (10x, High glucose, product NO. D2429), calcium sulfate dihydrate (ACS reagent, 98%, product NO. 255548). Laminin from Engelbreth-Holm-Swarm murine sarcoma basement membrane (product NO. L2020) were purchased from Sigma-Aldrich. Laminin (Red fluorescent, rhodamine, Cat.#LMN01-A) was purchased from Cytoskeleton, Inc.

Conductive hydrogel preparation: All hydrogel samples were based on 2% w/v alginate hydrogel. Pure alginate hydrogels were prepared by mixing 2.5% w/v sodium alginate and 183 mM CaSO₄ diluted in 1x dulbecco's modified eagle's media (DMEM). 0.8 ml of the 2.5% w/v sodium alginate and 0.2 ml of the 183 mM CaSO₄ were loaded into two separate syringes, and connected with female–female Luerlock connector. The solutions were mixed rapidly by pushing the syringes for approximately 6 times. Due to the fast gelation, the mixed solution was drop casted in 3D printed molds with controlled thickness and shape, and left for one hour to complete gelation. Alginate/PEDOT:PSS/Laminin hydrogel were prepared by mixing 22.5 mg sodium alginate and 563 μ L PEDOT:PSS with 90 μ L 10X DMEM and 237 μ L MiliQ H₂O. The mixture was left stirring overnight to ensure homogeneous mixing. 10 μ L laminin was then added in to the mixture and gently stirred in an ice bath to avoid laminin gelation. The solution was then loaded in a syringe and the hydrogels were casted using the same method as the pure alginate hydrogels.

Viscoelastic Properties by Oscillatory Rheology: The mechanical properties of the hydrogels were investigated with an AR 2000 rheometer. According to the hydrogel preparation method mentioned above, the hydrogel precursor was well-mixed with the calcium sulphate dispersion and directly loaded onto the Peltier plate (8 mm in diameter) of the rheometer for rheological analysis. After sample loading, the gap height was adjusted to 0.5 mm, and after gelation the temperature for all the measurements was maintained at 37 °C to simulate the cell culture condition. Strain sweeps were performed from 0.01 % to 100 % to determine the yield point and proper value setting for strain (Figure S2). The value of applied strain should be chosen before the yield point is reached, and should also fulfilled the premise of being able to apply sufficient stimulate to the samples. Here we select the value as 0.5 %. Oscillation-Time sweep under 0.5 % strain and 1 rad/s frequency was applied for 1 hour till the gelation process was completed. Next, an extra 15-minute Oscillation-Time sweep was performed to use the last set of data points as the storage modulus and loss modulus of the material. The dumping factor $\tan \delta$ can be calculated via the following equation:

equation 1:
$$\tan \delta = \frac{G''}{G'}$$

View Article Online DOI: 10.1039/D5TC02708J

Where G' is the storage modulus, G" is the loss modulus.

This article is licensed under a Creative Commons Attribution 3.0 Unported Licence

Open Access Article. Published on 28 Oktoba 2025. Downloaded on 17/11/2025 01:06:17.

Stress relaxation tests were measured first under 1% strain with 600 s duration, then under 1% strain for another 600 s.

Optical Transmittance Measurements: To ensure consistent results, all the samples for transmittance measurements were prepared by drop-casting onto glass substrates, which were controlled to thicknesses at 150, 400, and 1000 μm with 3D-printed spacers. Transmittance was measured using a LAMBDA UV/Vis spectrophotometer (PerkinElmer), with the incident light wavelengths ranging from 300 to 800 nm.

Electrochemical Characterization: All the measurements were performed with a PalmSens4 potentiostat at 37 °C in cell media. The experimental setup followed the standard three-electrode setup by using gold pogo pins (diameter=1.13 mm) integrated within a homemade 3D-printed mold with dimensions of width=5 mm* length=5 mm* height=10 mm (Figure S3) as working electrodes, a mesh Pt electrode (diameter=0.06 mm, open area=65%, 20 *20 mm) as the counter electrode and Ag/AgCl as the reference electrode. Prior to each measurement, all the samples were incubated in DMEM/F12 cell culture media and placed in the fridge to rest overnight. Electrochemical Impedance Spectroscopy (EIS) measurements were performed within the frequency range of 0.1 – 10⁵ Hz with an AC voltage perturbation of 10 mV at 0 V vs the reference electrode. Cyclic Voltammetry (CV) measurements were performed from -0.1 to 0.4 V under different scan rates 0.1 V/s, 0.2 V/s and 0.5 V/s. All the results presented here are extracted from at least three replicates for each condition and verified in many more experimental batches. The conductivity of the different systems studied was calculated by converting the resistance at 10⁵ Hz to conductivity using the flowing equation:³⁷

equation 2:
$$\sigma = \frac{A}{R*l}$$

Where A is the electrode surface (i.e. gold pogo pin diameter=1.13 mm * π * length=5 mm), I is the distance between working electrode and the counter electrode (i.e. 10 mm) and R is the resistance value extracted from the real impedance versus frequency plot (Figure S5) at different frequencies (i.e. 10^5 Hz for ionic conductivity and 0.1 Hz for electronic conductivity). The capacitance values from EIS were extracted directly from the impedance values at 0.1 Hz. The capacitance from cyclic voltammograms was calculated by integrating the current over the full potential range from the following equation:

equation 3:
$$C = \frac{\int I dv}{2*\Delta V * v}$$

Open Access Article. Published on 28 Oktoba 2025. Downloaded on 17/11/2025 01:06:17.

Where $\int I dv$ is the polygon area of the cyclic voltammogram, ΔV is the potential window and v is the potential window

equation 4:
$$f = \frac{v}{\Delta V}$$

where v = the scan rate and ΔV is the potential window, which was constant at 0.5 V in all of our studies (i.e. -0.1 V - 0.4 V).

SH-SY5Y human neuroblastomas-derived immature neuron-like cells: Prior to seeding onto the samples, human neuroblastoma SH-SY5Y cells (Sigma-Aldrich, #94030304) were maintained in Dulbecco's Modified Eagle Media/Nutrient Mixture F-12 (DMEM/F-12, 1:1; Thermo Fisher Scientific, #10565018) supplemented with 10% fetal bovine serum (FBS; Sigma-Aldrich, F7524) and 1% penicillin–streptomycin. Cells were cultured at 37 °C in a humidified atmosphere containing 5% CO₂. Upon reaching confluence, cells were detached using Accutase for 5 min, followed by centrifugation at 900 rpm for 5 min. The resulting cell suspension was seeded onto 24-well plates at a density of 10,000 cells/cm², with hydrogel samples (5 mm in diameter, 1 mm in thickness) placed in parallel wells, which were incubated with cell media the night before to ensure full swelling and absorption of cell media nutrients. After three days of culture, differentiation was induced by supplementing the media with 10 μM retinoic acid (Sigma-Aldrich, R2625) for an additional three days to promote the formation of immature neuron-like cells.

hiPSCs-derived Cortical Neuron Culture: Human induced pluripotent stem cell (hiPSC)-derived neural progenitor cells (NPCs; line SCTi003-A, StemCell Technologies, Catalog #200-0620) were thawed and cultured on Matrigel-coated 6-well plates for 4 days to allow expansion. Prior to cell seeding, wells of a 24-well plate were sequentially coated with poly-D-lysine (PDL; 0.1 mg/mL, 2 h at 37 °C; Gibco, #A38904-01) followed by laminin (100 μg/mL, 2 h at 37 °C; Sigma-Aldrich, #L2020). NPCs were seeded at a density of 50,000 cells per well, with hydrogel samples (5 mm in diameter, 1 mm in thickness) placed in parallel wells. Differentiation into cortical neurons was induced for 7 days using the STEMdiffTM Midbrain Neuron Differentiation Kit (StemCell Technologies, #100-0038). Subsequently, hiPSC-derived cortical neurons were maintained and matured in BrainPhysTM hiPSC Neuron Kit complete media (StemCell Technologies, #05795) supplemented with SM1, N2, brainderived neurotrophic factor (BDNF), glial cell line-derived neurotrophic factor (GDNF), ascorbic acid, and dibutyryl-cAMP, as provided in the kit. Cultures were maintained for the duration of the experiment with half-media changes every two days to promote neuronal maturation. All media were supplemented with 1% penicillin–streptomycin (Invitrogen, #15140122).

<u>Viability assay:</u> Viability assays were performed using the LIVE/DEADTM Cell Imaging Kit (488/570) from Thermo-fisher Scientific. Calcein AM, cell permeant dye was used as the live cell indicator (green)

and BOBO-3 Iodide was used as the dead cell indicator (red). The viability assay was performed vising colorons 1 μM calcein AM and 1 μL BOBO-3 Iodide in DMEM/F12 media. For both SH-SY5Y neuroblastomas cells and hiPSC-derived cortical neurons, the well plates were incubated for 15 min in a cell incubator with the reagents and respective culture media (DMEM/F12 media for the SH-SY5Y neuroblastomas cells and complete Brainphys media for the hiPSC-derived cortical neurons), then washed with PBS (x1) before topped up again with cell culture media. The well plates were directly imaged using a Keyence BZ-810 microscope system (Osaka, Japan).

Immunohistochemistry: At day in vitro 28 (DIV28), hiPSC-derived cortical neurons were fixed with 4% paraformaldehyde for 15 min at room temperature (RT) and subsequently permeabilized with 0.5% Triton X-100 (Sigma-Aldrich, St. Louis, MI, USA) in phosphate-buffered saline (PBS; Sigma-Aldrich) for 15 min. Following permeabilization, cells were washed three times with PBS for 5 min each at RT. To prevent non-specific antibody binding, samples were incubated with bovine serum albumin (BSA; Sigma-Aldrich, #9048468) for 30 min at RT, followed by three additional PBS washes (5 min each). Cells were then incubated with the primary antibody, mouse monoclonal anti-βIII-tubulin (2G10-TB3; eBioscienceTM, #14-4510-82; 0.5 mg/mL), diluted 1:100 in 1% BSA in Dulbecco's PBS (dPBS) for 1 h at RT. After washing, samples were incubated with the secondary antibody, goat anti-mouse Alexa Fluor 488 (Abcam, #ab150113), diluted 1:500 in 1% BSA in dPBS, for 1 h at RT in the dark. Finally, cell nuclei were counterstained with NucBlue (Life Technologies, Carlsbad, CA, USA) for 20 min. Fluorescence images were acquired using a Keyence BZ-810 microscope system (Keyence, Osaka, Japan).

Acknowledgements

LW and AS would like to thank Christina Tringides for fruitful discussions. LW and AS would like to thank Brian Nanhekhan and Chris S. Vink for support with research resources and infrastructure. The authors acknowledge funding from the Dutch Research Council (NWO) – grant no. NWA.1418.24.057. AS acknowledge financial support from the Sectorplan Beta II (2023), from the Dutch Ministry of Education, Culture and Science. MD and YH acknowledge Hypatia Grant (BoneChipPredict) from Radboud University Medical Center. JPF acknowledge the support from the Netherlands Organ-on- Chip Initiative, an NWO gravitation project funded by the Ministry of Education, Culture and Science of the government of the Netherlands (024.003.001).

References

This article is licensed under a Creative Commons Attribution 3.0 Unported Licence

Open Access Article. Published on 28 Oktoba 2025. Downloaded on 17/11/2025 01:06:17.

- Z. Lu, A. Pavia, A. Savva, L. Kergoat and R. M. Owens, *Elsevier Ltd*, 2023, preprint, DOI: View Article Online 10.1016/j.mser.2023.100726.
- D. T. Simon, E. O. Gabrielsson, K. Tybrandt and M. Berggren, *American Chemical Society*, 2016, preprint, DOI: 10.1021/acs.chemrev.6b00146.
- 3 C. Pitsalidis, A. M. Pappa, A. J. Boys, Y. Fu, C. M. Moysidou, D. van Niekerk, J. Saez, A. Savva, D. landolo and R. M. Owens, *American Chemical Society*, 2022, preprint, DOI: 10.1021/acs.chemrev.1c00539.
- 4 Z. Lu, D. van Niekerk, A. Savva, K. Kallitsis, Q. Thiburce, A. Salleo, A. M. Pappa and R. M. Owens, *J Mater Chem C Mater*, 2022, **10**, 8050–8060.
- D. Seidel, J. Obendorf, B. Englich, H. G. Jahnke, V. Semkova, S. Haupt, M. Girard, M. Peschanski, O. Brüstle and A. A. Robitzki, *Biosens Bioelectron*, 2016, **86**, 277–286.
- 6 F. Ravera, E. Efeoglu and H. J. Byrne, *Analyst*, 2024, **149**, 4041–4053.
- 7 B. M. Baker and C. S. Chen, 2012, preprint, DOI: 10.1242/jcs.079509.
- 8 J. Lou and D. J. Mooney, *Nature Research*, 2022, preprint, DOI: 10.1038/s41570-022-00420-7.
- 9 S. Kundu, M. E. Boutin, C. E. Strong, T. Voss and M. Ferrer, *Commun Biol*, DOI:10.1038/s42003-022-04177-z.
- 10 K. Y. Lee and D. J. Mooney, *Elsevier Ltd*, 2012, preprint, DOI: 10.1016/j.progpolymsci.2011.06.003.
- 11 X. Li, T. Liu, K. Song, L. Yao, D. Ge, C. Bao, X. Ma and Z. Cui, *Biotechnol Prog*, 2006, **22**, 1683–1689.
- 12 C. Gao, S. Song, Y. Lv, J. Huang and Z. Zhang, *John Wiley and Sons Inc*, 2022, preprint, DOI: 10.1002/mabi.202200051.
- C. M. Tringides, N. Vachicouras, I. de Lázaro, H. Wang, A. Trouillet, B. R. Seo, A. Elosegui-Artola, F. Fallegger, Y. Shin, C. Casiraghi, K. Kostarelos, S. P. Lacour and D. J. Mooney, *Nat Nanotechnol*, 2021, **16**, 1019–1029.
- 14 L. T. A. Hong, Y. M. Kim, H. H. Park, D. H. Hwang, Y. Cui, E. M. Lee, S. Yahn, J. K. Lee, S. C. Song and B. G. Kim, *Nat Commun*, DOI:10.1038/s41467-017-00583-8.
- 15 C. M. Tringides, M. Boulingre, A. Khalil, T. Lungjangwa, R. Jaenisch and D. J. Mooney, *Adv Healthc Mater*, DOI:10.1002/adhm.202202221.
- 16 R. Borah, J. O'Sullivan, M. Suku, D. Spurling, D. Diez Clarke, V. Nicolosi, M. A. Caldwell and M. G. Monaghan, *J Biomed Mater Res A*, DOI:10.1002/jbm.a.37859.
- 17 K. Sagdic, E. Fernández-Lavado, M. Mariello, O. Akouissi and S. P. Lacour, *Springer Nature*, 2023, preprint, DOI: 10.1557/s43577-023-00536-1.
- L. Sifringer, L. De Windt, S. Bernhard, G. Amos, B. Clément, J. Duru, M. W. Tibbitt and C. M. Tringides, *J Mater Chem B*, DOI:10.1039/d4tb00807c.
- 19 Y. Ahn, H. Lee, D. Lee and Y. Lee, ACS Appl Mater Interfaces, 2014, 6, 18401–18407.

- H. Li, J. Cao, R. Wan, V. R. Feig, C. M. Tringides, J. Xu, H. Yuk and B. Lu, *John Wiley and Son Strong Tollow* 2024, preprint, DOI: 10.1002/adma.202415151.
- H. Montazerian, E. Davoodi, C. Wang, F. Lorestani, J. Li, R. Haghniaz, R. R. Sampath, N. Mohaghegh, S. Khosravi, F. Zehtabi, Y. Zhao, N. Hosseinzadeh, T. Liu, T. K. Hsiai, A. H. Najafabadi, R. Langer, D. G. Anderson, P. S. Weiss, A. Khademhosseini and W. Gao, *Nat Commun*, 2025, **16**, 3755.
- A. R. Spencer, A. Primbetova, A. N. Koppes, R. A. Koppes, H. Fenniri and N. Annabi, *ACS Biomater Sci Eng*, 2018, **4**, 1558–1567.
- A. P. Goestenkors, T. Liu, S. S. Okafor, B. A. Semar, R. M. Alvarez, S. K. Montgomery, L. Friedman and A. L. Rutz, *J Mater Chem B*, 2023, **11**, 11357–11371.
- A. Savva, J. Saez, A. Withers, C. Barberio, V. Stoeger, S. Elias-Kirma, Z. Lu, C. M. Moysidou, K. Kallitsis, C. Pitsalidis and R. M. Owens, *Mater Horiz*, 2023, **10**, 3589–3600.
- C. Barberio, J. Saez, A. Withers, M. Nair, F. Tamagnini and R. M. Owens, *Adv Healthc Mater*, DOI:10.1002/adhm.202200941.
- T. C. Tseng, L. Tao, F. Y. Hsieh, Y. Wei, I. M. Chiu and S. H. Hsu, *Advanced Materials*, 2015, 27, 3518–3524.
- D. T. Wu, M. Diba, S. Yang, B. R. Freedman, A. Elosegui-Artola and D. J. Mooney, *Bioeng Transl Med*, DOI:10.1002/btm2.10464.
- 28 K. Y. Lee and D. J. Mooney, *Elsevier Ltd*, 2012, preprint, DOI: 10.1016/j.progpolymsci.2011.06.003.
- 29 G. Chan and D. J. Mooney, *Acta Biomater*, 2013, **9**, 9281–9291.
- O. Chaudhuri, J. Cooper-White, P. A. Janmey, D. J. Mooney and V. B. Shenoy, *Nature*, 2020, 584, 535–546.
- 31 D. T. Wu, N. Jeffreys, M. Diba and D. J. Mooney, *Tissue Eng Part C Methods*, 2022, **28**, 289–300.
- O. Chaudhuri, L. Gu, D. Klumpers, M. Darnell, S. A. Bencherif, J. C. Weaver, N. Huebsch, H. Lee, E. Lippens, G. N. Duda and D. J. Mooney, *Nat Mater*, 2016, **15**, 326–334.
- D. T. Wu, M. Diba, S. Yang, B. R. Freedman, A. Elosegui-Artola and D. J. Mooney, *Bioeng Transl Med*, 2023, **8**, e10464.
- O. Chaudhuri, J. Cooper-White, P. A. Janmey, D. J. Mooney and V. B. Shenoy, *Nature*, 2020, **584**, 535–546.
- 35 A. Saha, A. Mal, A. Elgendy, D. G. Marangoni and S. Ghosh, *Can J Chem*, DOI:10.1139/cjc-2024-0245.
- R. E. Daso, R. Posey, H. Garza, A. Perry, C. Petersen, A. C. Fritz, J. Rivnay and J. Tropp, *Adv Funct Mater*, 2025, **n/a**, e08859.
- A. Ch. Lazanas and M. I. Prodromidis, ACS Measurement Science Au, 2023, 3, 162–193.
- 38 C. Barberio, J. Saez, A. Withers, M. Nair, F. Tamagnini and R. M. Owens, *Adv Healthc Mater*, 2022, **11**, 2200941.

J. A. Rowley, G. Madlambayan and D. J. Mooney, *Biomaterials*, 1999, **20**, 45–53. View Article Online

21

 July 16th 2025
 View Article Online

 DOI: 10.1039/D5TC02708J

On behalf of all the co-authors, we are declaring that the data supporting the manuscript entitled "Electrically Active Hydrogels based on PEDOT:PSS For Neural Cultures" have been included as part of the Supplementary Information.

Yours sincerely,

Dr. Achilleas Savva